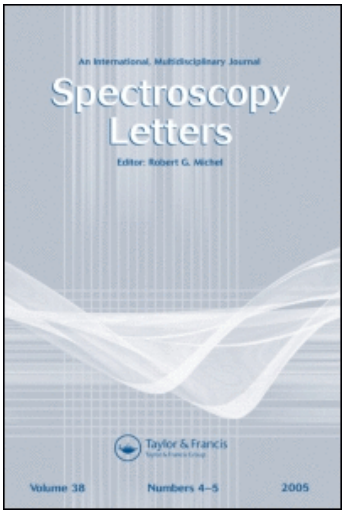

Spectroscopy Letters
Publication details, including instructions for authors and subscription information:
http://www.informaworld.com/smpp/title~content=t713597299

Downconversion for Solar Cells in $YF_3:Pr^{3+}$, Yb^{3+}

Linda Aarts[a]; Bryan van der Ende[ab]; Michael F. Reid[c]; Andries Meijerink[a]
[a] Condensed Matter and Interfaces, Debye Institute for Nanomaterials Science, Utrecht University, Utrecht, The Netherlands [b] Department of Physics and Astronomy, Trent University, Peterborough, Ontario, Canada [c] Department of Physics and Astronomy, University of Canterbury, Christchurch, New Zealand

Online publication date: 30 July 2010

To cite this Article Aarts, Linda , Ende, Bryan van der , Reid, Michael F. and Meijerink, Andries(2010) 'Downconversion for Solar Cells in $YF_3:Pr^{3+}$, Yb^{3+}', Spectroscopy Letters, 43: 5, 373 — 381
To link to this Article: DOI: 10.1080/00387010.2010.486731
URL: http://dx.doi.org/10.1080/00387010.2010.486731

Spectroscopy Letters, 43:373–381, 2010

ISSN: 0038-7010 print/1532-2289 online
DOI: 10.1080/00387010.2010.486731

Taylor & Francis
Taylor & Francis Group

Downconversion for Solar Cells in YF_3:Pr^{3+}, Yb^{3+}

Linda Aarts[1], Bryan van der Ende[1,2], Michael F. Reid[3], and Andries Meijerink[1]

[1]Condensed Matter and Interfaces, Debye Institute for Nanomaterials Science, Utrecht University, Utrecht, The Netherlands
[2]Department of Physics and Astronomy, Trent University, Peterborough, Ontario, Canada
[3]Department of Physics and Astronomy, University of Canterbury, Christchurch, New Zealand

ABSTRACT Energy losses in solar cells caused by the spectral mismatch can be reduced by adapting the solar spectrum using a downconversion material where *one* higher energy visible photon is 'cut' into *two* lower energy near-infrared photons that both can be absorbed by the solar cell. Downconversion with the (Pr^{3+}, Yb^{3+}) couple in YF_3 is investigated. Based on analysis of luminescence and diffuse reflectance spectra it is evident that two-step energy transfer takes place from the $^3P_0$ level of Pr^{3+} (around 490 nm) exciting two Yb^{3+} to the $^2F_{5/2}$ level giving emission around 980 nm. The transfer efficiency increases with Yb^{3+} concentration and is 86% for YF_3 doped with 0.5% Pr^{3+} and 30% Yb^{3+}. Due to concentration quenching the intensity of emission from Yb^{3+} is strongly reduced and the $^2F_{5/2}$ emission intensity reaches a maximum for the sample with 0.5% Pr^{3+} and 2–5% Yb^{3+} at 300 K. Temperature dependent measurements reveal the role of the Pr^{3+} $^1G_4$ level in the energy transfer between Pr^{3+} and Yb^{3+}. Back-transfer of excitation energy from the Yb^{3+} $^2F_{5/2}$ level to the $^1G_4$ level of Pr^{3+} occurs and quenches the Yb^{3+} emission. The quenching is shown to become more efficient between 4 and 50 K due to faster phonon-assisted energy transfer between the Yb^{3+} donors. Upon raising the temperature from 50 to 300 K, the luminescence life time of the Yb^{3+} emission increases again because the small energy difference between the Pr^{3+} ($^1G_4$) level and the Yb^{3+} ($^2F_{5/2}$) level ($\sim$300 cm^{-1}) which makes the $^1G_4$ less efficient as a trap for the excitation energy. The present results give insight into factors involved in the concentration quenching in downconversion materials based on the (Pr^{3+}, Yb^{3+}) couple.

KEYWORDS downconversion/quantum cutting, lanthanides, luminescence, photovoltaics

1. INTRODUCTION

The theoretical maximum energy conversion efficiency of solar cells is 30%; this is known as the Shockley-Queisser limit.[1] The major part of the losses is related to the spectral mismatch: photons with an energy smaller than the bandgap (E_g) cannot be absorbed (sub-bandgap transmission) and a large part of the energy of photons with an energy larger than the bandgap is lost as heat (thermalization losses). The energy losses related

Address correspondence to Andries Meijerink, Condensed Matter and Interfaces, Debye Institute for Nanomaterials Science, Utrecht University, Princetonplein 5, Utrecht 3584 CC, The Netherlands. E-mail: a.meijerink@uu.nl

to the spectral mismatch can be reduced adapting the solar spectrum before it is absorbed by the solar cell. One option is to add two lower-energy photons (that are otherwise transmitted) to obtain one photon with an energy large enough so that it can be absorbed by the solar cell. This process is known as upconversion (UC) and is well suited for solar cells with a large band-gap where transmission losses dominate. A second option is to split one higher energy photon to obtain two photons with a smaller energy. Each of these photons can subsequently be absorbed by the solar cell and can generate an electron-hole pair. This is known as downconversion (DC) and is most beneficial for solar cells with a smaller band-gap where thermalization losses are the major loss factor. The theoretical limit for the conversion efficiency can be increased from 30% to 39% by applying an ideal downconverting layer on top of a c-Si solar cell.[1] Downconversion is also known as quantum cutting because one photon is 'cut' into two smaller energy photons. Lanthanide ions are very well suited to use for DC or UC because they have a rich energy level structure that allows for efficient spectral conversion. There are many examples of efficient up- and downconversion using lanthanides, either with one type of lanthanide ion or with pairs of lanthanide ions.[2,3]

Initial work on downconversion materials was aimed at the conversion of one vacuum UV photon in two visible photons.[3–6] Cascade emission from the $^1S_0$ level of Pr^{3+} or two-step energy transfer in the (Gd^{3+}, Eu^{3+}) couple has shown efficient VUV to VIS conversion.[3–6] The realization that the downconversion concept can also be used to boost the efficiency in solar cells, triggered research on downconversion in lanthanide doped materials. Downconversion of visible photons into NIR photons has been first demonstrated in (Y, Yb) PO_4:Tb^{3+}.[7] After excitation into the $^5D_4$ state of the Tb^{3+}-ion two neighboring Yb^{3+} ions are excited through a cooperative energy transfer process. More recently, cooperative downconversion has also been reported for (Tb^{3+}, Yb^{3+}) in other host lattices[8,9] and for other lanthanide couples, viz. (Pr^{3+}, Yb^{3+})[10] and (Tm^{3+}, Yb^{3+}),[11] although it is not clear that the second-order cooperative energy transfer process is the operative mechanism in the latter two systems as also first-order energy transfer processes are possible and are expected to dominate.[12]

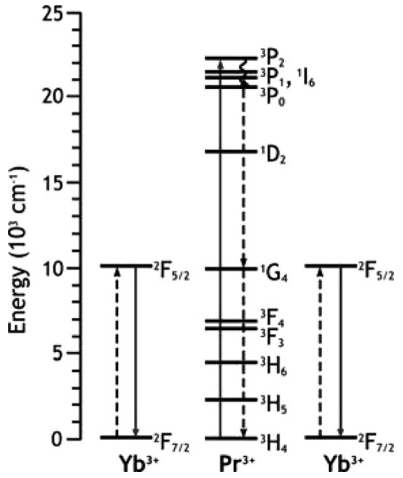

FIGURE 1 **Schematic representation of the downconversion mechanism for the (Pr^{3+}, Yb^{3+}) couple. Pr^{3+} is excited into the ^3P_J state. Part of the energy is donated to Yb^{3+} via cross relaxation: Pr^{3+} ($^3P_0 \rightarrow {}^1G_4$), Yb^{3+} ($^2F_{7/2} \rightarrow {}^2F_{5/2}$), populating the $^2F_{5/2}$ level of Yb^{3+}. In the second step the remaining energy can be transferred to a second Yb^{3+}-ion from the $^1G_4$ level of Pr^{3+}. Both Yb^{3+}-ions can then emit a photon of approximately 1000 nm.**

In a recent paper we presented evidence for efficient downconversion with the (Pr^{3+}, Yb^{3+}) couple in SrF_2.[12] Figure 1 shows the downconversion scheme via sequential two-step energy transfer. When Pr^{3+} is excited into the $^3P_0$ state part of the energy is donated to Yb^{3+} via cross relaxation: Pr^{3+} ($^3P_0 \rightarrow {}^1G_4$), Yb^{3+} ($^2F_{7/2} \rightarrow {}^2F_{5/2}$), populating the $^2F_{5/2}$ level of Yb^{3+}. In a second step the remaining energy can be transferred to a second Yb^{3+}-ion, which can then emit a photon. In SrF_2 the lanthanide ions form clusters[13,14] due to the need for charge compensation (Pr^{3+} or Yb^{3+} replaces Sr^{2+}). The clustering will influence the energy transfer between Pr^{3+} and Yb^{3+}. In the YF_3 host lattice, the lanthanides replace the chemically similar Y^{3+} ions and will therefore be randomly distributed through the lattice. In this chapter we investigate if efficient downconversion is also possible with the (Pr^{3+}, Yb^{3+}) couple in the YF_3 host lattice and detailed studies on the temperature dependence of the energy transfer processes are reported to gain further insight in the mechanism and kinetics of the energy transfer processes influencing the downconversion efficiency.

2. EXPERIMENTAL

2.1. Synthesis

Crystalline powder samples of YF_3 doped with Pr^{3+} and Yb^{3+} were synthesized via co-precipitation

followed by high temperature sintering. The samples were prepared by mixing stoichiometric amounts of Y_2O_3, Pr_2O_3, and Yb_2O_3 (purity at least 4N). In all cases the percentages of Pr^{3+} and Yb^{3+} are atomic percentage (or mole%) relative to Y^{3+}. The powder mixture was dissolved in dilute hydrochloric acid. Typically, 3 to 5 mL of concentrated acid was heated, and after the oxides had dissolved it was diluted to 100 mL with deionized water. After adding 100 ml of solution with an excess of NH_4F (98+%) a fluoride precipitate was formed, which was centrifuged and washed three times with 100 mL of deionized water and then dried at 120°C for several hours. The mixture was put into an alumina crucible and fired in an oven together with an excess of NH_4F (added by mixing in a mortar) under a nitrogen flow. The samples were first heated to 300°C for two hours (to remove adsorbed water molecules) and then to the reaction temperature of 1000°C for 3 hours. After the samples had cooled sufficiently they were crushed with a pestle and mortar and x-ray diffraction measurements were performed to check for phase purity.

2.2. Measurements

Diffuse reflectance spectra were measured with a Perkin-Elmer Lambda 950 UV/VIS/IR absorption spectrometer. Emission and excitation measurements were performed using an Edinburgh Instruments FLS920 fluorescence spectrometer with a 450 W Xe lamp as excitation source, a 0.3 m excitation double monochromator and two emission monochromators to record emission spectra in the wavelength range 250 to 800 nm (with a Hamamatsu R928 photomultiplier tube) or in the wavelength range 800 to 1700 nm (with a liquid nitrogen-cooled Hamamatsu R5509-72 PMT). The Edinburgh fluorescence spectrometer is equipped with an Oxford helium flow cryostat for low temperature measurements. The spectra were not corrected for the instrumental response, unless otherwise indicated.

Luminescence decay curves were recorded using of a Lambda Physik LPD3000 tunable dye laser using a Coumarin 120 dye solution (tunable between 423 and 462 nm) or a Stryryl 14 dye solution (tunable between 904 and 992 nm). The laser is pumped by a Lambda Physik LP × 100 excimer (XeCl) laser. The typical pulse width for the setup is ~20 ns and the repetition rate is 10 Hz. The laser excitation is steered into the sample chamber of the Edinburgh fluorescence spectrometer using a pair of prisms and decay curves are recorded with a multi-channel scaling card.

3. RESULTS AND DISCUSSION

3.1. Characterization

Samples of YF_3 doped with 0.5% Pr^{3+} and 0, 2, 3, 4, 5, 10, and 30% Yb^{3+} and one sample doped with 5% Yb^{3+} and no Pr^{3+} were synthesized. X-ray diffraction measurements for all samples are consistent with the orthorhombic structure of YF_3.

Diffuse reflectance spectra were recorded to confirm if Pr^{3+} and Yb^{3+} were incorporated into the host-lattice. From the diffuse reflectance spectra (Fig. 2) it can be concluded that both Pr^{3+} and Yb^{3+} are present in the samples. The absorption strengths for the peaks corresponding to Pr^{3+} absorptions (e.g., the $^3H_4 \rightarrow {}^3P_J$ transitions between 440 and 490 nm) differ from sample to sample, even though in the starting mixture the same amount of Pr^{3+} (0.5 mole%) was present. This shows that the incorporation of Pr^{3+} varied between samples, probably related to the larger ionic radius of Pr^{3+} in comparison to Yb^{3+}. Also the fluoride precipitation step where the Pr^{3+} is incorporated in the YF_3 may have resulted in differences in the amount of Pr^{3+} incorporated in the fluoride, which will be especially notable for Pr^{3+} ion due to the low

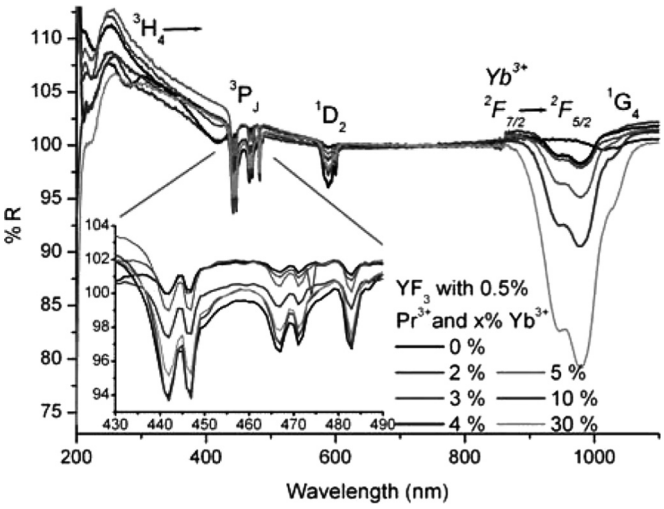

FIGURE 2 **Diffuse reflection spectra of YF_3 doped with 0.5% Pr^{3+} and up to 30% Yb^{3+} recorded at 300 K.**

(0.5%) concentration. For the present study involving energy transfer from the Pr^{3+} donor to the Yb^{3+} acceptor the variation in the donor concentration will not affect the conclusions as the acceptor concentration determines the transfer dynamics. The peak for the Yb^{3+} absorption ($^2F_{7/2} \rightarrow {}^2F_{5/2}$ transition) around 1000 nm does vary in good agreement with the Yb^{3+} concentration.

3.2. Room Temperature Luminescence

In Fig. 3, emission spectra are shown for YF_3 doped with 0.5% Pr^{3+} and between 0 and 30 mole% Yb^{3+} after excitation into the Pr^{3+} $^3P_2$ state (446 nm). When no Yb^{3+} is present only emission from the $^3P_0$ (e.g., $^3P_0 \rightarrow {}^3H_4$ emission at 482 nm and $^3P_0 \rightarrow {}^3H_6$ emission at 604 nm) level is observed. The spectrum is similar to previously reported emission spectra for Pr^{3+} in YF_3.[15] Upon excitation in the $^3P_2$ level, fast relaxation to the $^3P_0$ level takes place followed by emission to the various lower energy levels of Pr^{3+}. There is no evidence for $^1D_2$ emission, consistent with the relatively large energy gap between $^3P_0$ and $^1D_2$ (3500 cm^{-1}) and the low maximum phonon energy in YF_3 (500 cm^{-1})[15] which makes multiphonon relaxation from $^3P_0$ to $^1D_2$ a very slow process (7 or more phonon emission).

In the infrared region several Pr^{3+} emission bands are observed. The emission band around 900 nm is assigned to the $^3P_0 \rightarrow {}^1G_4$ transition. This populates the $^1G_4$ level and emission from the $^1G_4$ level is observed around 1030 nm (very weak) due to the $^1G_4 \rightarrow {}^3H_4$ transition and around 1320 nm due to the $^1G4 \rightarrow {}^3H_5$ transition. Note that the reverse transition $^3H_4 \rightarrow {}^1G_4$ can be observed as weak absorption lines around 1020 nm in Fig. 2. To understand the intensity distribution for the emission from the $^1G_4$ level, Table 1 gives the squared reduced matrix elements for the various transitions originating from the $^1G_4$ level. The reduced matrix elements were calculated using the programs developed by Reid and Burdick.[16] Transition probabilities from the $^1G_4$ level can now determined using the Judd-Ofelt theory.[17] The transition strength S (in cm^2) is given by

$$S - \sum_{t=2,4,6} \Omega_t |\langle aj|U^{(t)}|bj'\rangle|^2 \qquad (1)$$

where Ω_t are the Judd-Ofelt intensity parameters that depend on the host-lattice and the doubly reduced matrix elements of the unit tensor operator $U^{(t)}$ can be calculated for transitions between different multiplets (indicated by aj and bj' in Eq. (1)).[16] In Table I the squared reduced matrix elements $|\langle aj|U^{(t)}|bj'\rangle|$ (abbreviated as $U^{(t)}$) are given for transitions from the $^1G_4$ level of Pr^{3+}. The table shows that, compared to the total $^1G_4$ emission intensity, the contribution of the $^1G_4 \rightarrow {}^3H_4$ transition is 0.38% for $U^{(2)}$, 1.2% for $U^{(4)}$ and 2.1% for $U^{(6)}$. The emission from the $^1G_4$ level will be dominated by transitions to the $^3H_5$, $^3H_6$ and $^3F_4$ levels and the $^1G_4 \rightarrow {}^3H_4$ emission will be weak, for any set of Judd-Ofelt parameters. Note that the two-step emission from the $^3P_0$ level via the $^1G_4$ level is, in fact, a viable route for quantum cutting of one

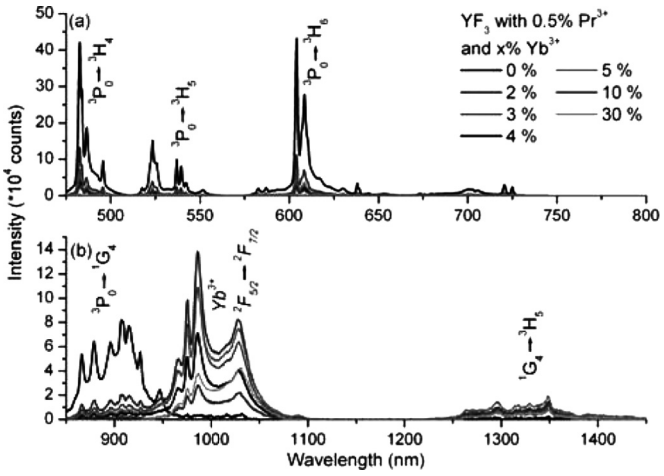

FIGURE 3 **Room temperature emission spectra for the visible (a) and infrared (b) part of the spectrum for YF_3:Pr^{3+} (0.5%), Yb^{3+} (0, 2, 3, 4, 5, 10, and 30%). The intensity for the visible and IR part of the spectrum cannot be compared since these were measured with different detectors. The excitation wavelength is 446 nm ($^3P_2$ level).**

TABLE 1 **Reduced Matrix Elements $(U^{(t)})^2$ for Transition Starting from the $Pr^{3+}{}^1G_4$ Level**

Transition	$(U^{(2)})^2$	$(U^{(4)})^2$	$(U^{(6)})^2$
$^1G_4 \rightarrow {}^3H_4$	0.00141	0.00635	0.02206
$^1G_4 \rightarrow {}^3H_5$	0.03739	0.09615	0.41314
$^1G_4 \rightarrow {}^3H_6$	0.25226	0.25337	0.23683
$^1G_4 \rightarrow {}^3F_2$	0.00004	0.01580	0.00587
$^1G_4 \rightarrow {}^3F_3$	0.00381	0.00531	0.05173
$^1G_4 \rightarrow {}^3F_4$	0.07819	0.14271	0.34419
Sum	0.37310	0.51968	1.07382
Percentage ($^1G_4 \rightarrow {}^3H_4$)	0.38	1.2	2.1

The percentages in the bottom row give the $(U^{(t)})^2$ strength for the $^1G_4 \rightarrow {}^3H_4$ transitions relative to the sum of all $(U^{(t)})^2$ values for a given value of *t*.

blue/green photon into two infrared photons, but the efficiency for generating 1000 nm photons is very low. Especially for the second step, the percentage of useful (for c-Si solar cells) IR photons around 1000 nm is low, around 1%, while ~99% of the photons will be emitted at wavelengths that are too long to be absorbed by c-Si.

When Yb^{3+} is added as a co-dopant, the intensity of the Pr^{3+} $^3P_0$ emission decreases. Already for 2% of Yb^{3+} a significant drop is observed. Around 1000 nm new emission peaks appear, which are assigned to $^2F_{5/2} \rightarrow {}^2F_{7/2}$ transitions on Yb^{3+}. In addition, emission around 1320 nm is present, which is assigned to the Pr^{3+} $^1G_4 \rightarrow {}^3H_5$ transition. This shows that there is efficient energy transfer from Pr^{3+} to Yb^{3+}, consistent with the first energy transfer step depicted in Fig. 1 resulting in population of the $^2F_{5/2}$ level of Yb^{3+} and the $^1G_4$ level of Pr^{3+}. As the Yb^{3+} concentration is increased the Pr^{3+} $^3P_0$ emission continues to decrease, and it has almost completely disappeared for the sample co-doped with 0.5% Pr^{3+} and 30% Yb^{3+}. Based on the emission spectra shown in Fig. 3(b) and diffuse reflectance spectra in Fig. 2, it is not surprising that energy transfer is efficient: there is good spectral overlap between the $^3P_0 \rightarrow {}^1G_4$ emission, which extends beyond 950 nm, and the Yb^{3+} absorption band (Fig. 2). The intensity of the Yb^{3+} emission reaches a maximum for the sample co-doped with 0.5% Pr^{3+} and 2% to 5% Yb^{3+} and then starts to decrease. The strong decrease of the Yb^{3+} emission intensity in the samples co-doped with 10% and 30% Yb^{3+} is ascribed to concentration quenching. This commonly observed for concentrated lanthanide compounds. Energy transfer between neighboring Yb^{3+} ions leads to energy migration to traps and quenching centers and explains the lower Yb^{3+} emission intensity in the compounds with high Yb^{3+} concentrations.

To gain further insight in the energy transfer process between Pr^{3+} and Yb^{3+}, luminescence decay curves were recorded for the $^3P_0$ emission from Pr^{3+} and the $^2F_{5/2}$ emission from Yb^{3+} upon excitation into the Pr^{3+} ^3P_J levels. Figures 4 and 5 show room temperature luminescence decay curves of these emissions for YF_3 doped with 0.5% Pr^{3+} and co-doped with 0% to 30% Yb^{3+} for Pr^{3+} $^3P_0$ emission at 604 nm and Yb^{3+} $^2F_{5/2}$ emission at 986 nm. Apart from a small deviation in the beginning of the curve, probably due to energy transfer to defects, a single

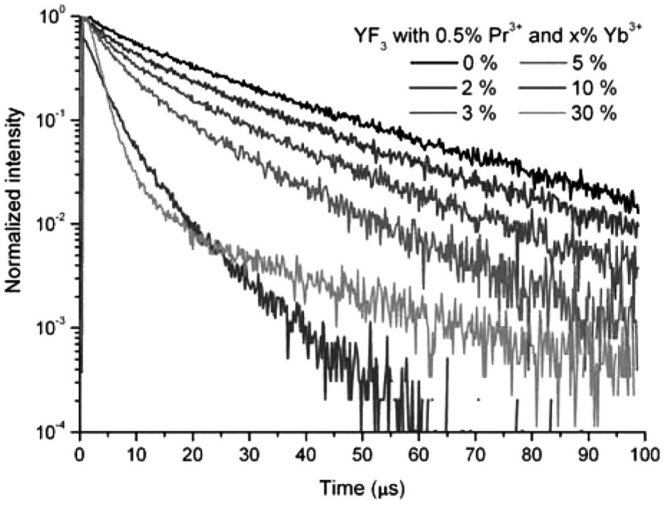

FIGURE 4 **Room temperature luminescence decay measurements of the Pr^{3+} $^3P_0$ emission (604 nm) in YF_3:Pr^{3+} (0.5%), Yb^{3+} (0, 2, 3, 5, 10, and 30%) after pulsed excitation into the Pr^{3+} $^3P_2$ level (442 nm).**

exponential decay is observed for Pr^{3+} $^3P_0$ emission in YF_3:Pr^{3+}(0.5%) with a decay time of 25 μs (Fig. 4). This value is consistent with radiative life times reported for the $^3P_0$ emission in this and similar (fluoride) host lattices.[18,19] Addition of Yb^{3+} results in a decrease of the lifetime and the decay becomes non-exponential, due to energy transfer from Pr^{3+} to Yb^{3+}. The decay curves recorded for the Pr^{3+} emission for the different concentrations show a clear decrease in the luminescence decay time upon raising the Yb^{3+} concentration. Especially for the highest concentrations (10% and 30% Yb^{3+}) a fast

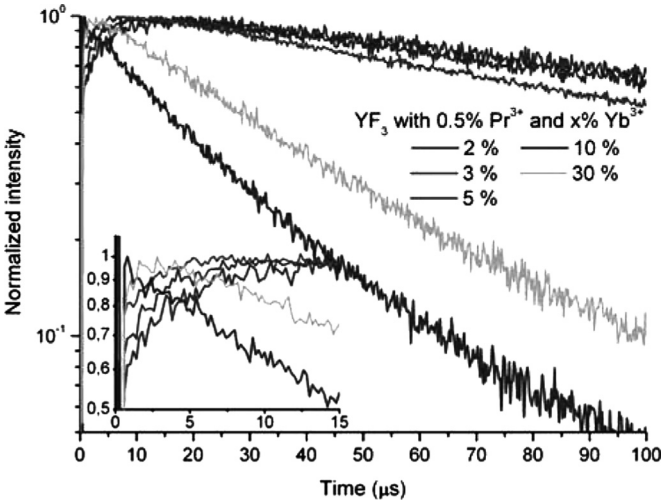

FIGURE 5 **Room temperature luminescence decay measurements of Yb^{3+} $^2F_{5/2}$ emission (986 nm) in YF_3:Pr^{3+} (0.5%), Yb^{3+} (2, 3, 5, 10, and 30%) after excitation into the Pr^{3+} $^3P_2$ level (442 nm). The inset shows the build-up in the first 15 μs of the decay curve.**

decay is observed, consistent with the large intensity drop observed for these concentrations. The non-exponential character of the decay curves reflects the different distributions of Yb^{3+} acceptor ions around a Pr^{3+}-ion, leading to a variety of energy transfer rates for different Pr^{3+} ions. Even though the luminescence decay curves of the co-doped samples are not two-exponential, they can be fitted with a two-exponential function to obtain an estimate of the lifetime of Pr^{3+} $^3P_0$ emission and the efficiency of the energy transfer processes as a function of the Yb^{3+} concentration. The lifetime τ determined for the slower component decreases from 25 μs for the sample without Yb^{3+} to 11 μs for the sample with the highest Yb^{3+} concentration. The decay times determined for the faster component decrease from 6.0 μs for the sample co-doped with 2% Yb^{3+} to 2.6 μs when 30% Yb^{3+} is present in the sample, indicating that energy transfer becomes more efficient at higher Yb^{3+} concentrations. The overall energy transfer efficiency, i.e., the fraction of Pr^{3+} ions that relax through energy transfer instead of radiative decay, can be obtained from the integrals under the normalized decay curves.[7] From the decay curves in Fig. 4 the energy transfer efficiency from the $^3P_0$ level was estimated to be 25, 44, 59, 85 and 86% for co-doping with 2, 3, 5, 10, and 30% Yb^{3+}, respectively. This shows that downconversion is efficient already at relatively low Yb^{3+} concentrations. In comparison with SrF_2:Pr^{3+}, Yb^{3+} the efficiency is however lower: at 5% Yb^{3+} the transfer efficiency was already 77% and at 17% Yb^{3+} a 99% transfer efficiency was observed.[12] The higher transfer efficiency in SrF_2:Pr^{3+}, Yb^{3+} is explained by clustering of the lanthanides.

The luminescence decay curves for Yb^{3+} $^2F_{5/2}$ emission in Fig. 5 were fitted to a two-exponential function with a feeding term (with characteristic time τ_1) and a decay term (with a decay time τ_2). In this case τ_1 represents the build-up that is visible in the first 15 μs of the decay, and τ_2 is the lifetime of the Yb^{3+} $^2F_{5/2}$ emission. The build-up is caused by feeding of the Yb^{3+} $^2F_{5/2}$ emission by energy transfer from Pr^{3+}. The build-up becomes faster as more Yb^{3+} is added to the sample, decreasing from 5.4 μs for 2% Yb^{3+} to 1.0 μs for 30% Yb^{3+}. These numbers are consistent with the fast lifetime component of the $^3P_0$ emission and confirm that the build-up is due to feeding of Yb^{3+} $^2F_{5/2}$ level by energy transfer from the $^3P_0$ level with transfer rates up to 10^6 for the highest Yb^{3+} concentrations. The lifetime of the Yb^{3+}($^2F_{5/2}$) emission is given by the decay term and decreases from 147 μs to 36 μs when the Yb^{3+} concentration is increased from 2% to 30%. At higher Yb^{3+} concentrations concentration quenching leads to a shorter emission lifetime. The effect of concentration quenching is also observed in emission spectra (Fig. 3).

Convincing evidence for the occurrence of downconversion can be obtained from excitation and reflectance spectra. By comparing diffuse reflectance and excitation spectra which are corrected for the instrumental response (Fig. 6) the downconversion efficiency can be estimated as outlined by van der Ende et al.[12] The method relies on the fact that downconversion from the $^3P_0$ level leads to excitation of two Yb^{3+}-ions while one-step energy transfer from the $^1D_2$ feeds only one Yb^{3+}-ion. As a result, the ratio of the $^3P_J/^1D_2$ lines is expected to be two times higher in the excitation spectrum in comparison to the diffuse reflection spectrum. Since the energy transfer is complete at an Yb^{3+} concentration of 30%, this sample was selected for a comparison of the diffuse reflectance and excitation spectra. From the diffuse reflectance spectrum the ratio of the total absorption (integrated spectral area) of the $^3H_4 \rightarrow {}^3P_J$ and $^3H_4 \rightarrow {}^1I_6$ transitions relative to that of the

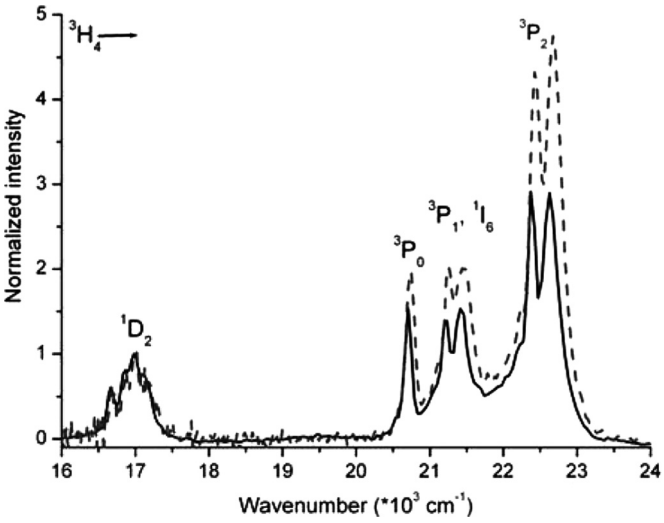

FIGURE 6 **Diffuse reflectance (*solid black line*) and excitation (dotted red line) spectra for YF_3:Pr^{3+} (0.5%), Yb^{3+} (30%), demonstrating that quantum cutting takes place. Both spectra are normalized at the peak of the $^1D_2$ emission (17000 cm^{-1}). The excitation spectrum monitored Yb^{3+} emission at 980 nm, and was corrected for wavelength-dependent instrument response.**

$^3H_4 \rightarrow {}^1D_2$ transition was determined to be 5.5. After correcting the excitation spectrum for wavelength-dependent instrumental response the ratio for the same transitions in the excitation spectrum of the Yb^{3+} emission was 8.9. This ratio is close to twice the value of that of the ratio found from diffuse reflectance, confirming that absorption of a photon into the ^3P_J and $^1I_6$ levels results in excitation of two Yb^{3+} ions.

3.3. Temperature-Dependent Measurements

To obtain a better insight in the energy transfer processes involved in downconversion and concentration quenching in the Pr^{3+}-Yb^{3+} system, temperature dependent luminescence measurements and life time measurements were performed between 4 and 300 K. Energy losses related to concentration quenching reduce the overall downconversion efficiency and insight in the energy transfer processes can aid in optimizing the luminescence efficiency. An important aspect in the case of the (Pr^{3+}, Yb^{3+}) downconversion couple is that the Pr^{3+} ions not only acts as donor (energy transfer from the $^3P_0$ level of Pr^{3+}) but can also trap the excitation from Yb^{3+} ions in the excited $^2F_{5/2}$ state as the lowest energy $^1G_4$ crystal field (CF) component is some 300 cm^{-1} lower in energy than the lowest energy CF component of the $^2F_{5/2}$ state. As discussed above, the reduced matrix elements for the various transitions (Table I) show that the strongest emissions from the $^1G_4$ state are not to the $^3H_4$ ground state, but to the $^3H_5$, $^3H_6$, and $^3F_3$ levels giving emission around 1320, 1840 and 2900 nm, respectively. Clearly, these emissions are not useful for c-Si solar cells. To study the influence of concentration quenching, emission spectra were recorded as a function of temperature under direct excitation into the $^2F_{5/2}$ excited state of Yb^{3+} (986 nm). The emission spectra for some representative temperatures are shown in Fig. 7. At 4 K relatively strong and narrow emission lines are observed. Between 4 and 20 K the intensity drops rapidly. Above 50 K the intensity recovers and at room temperature the intensity is similar to that at 4 K. In addition, line broadening is observed due fast phonon-induced dephasing processes at elevated temperatures.

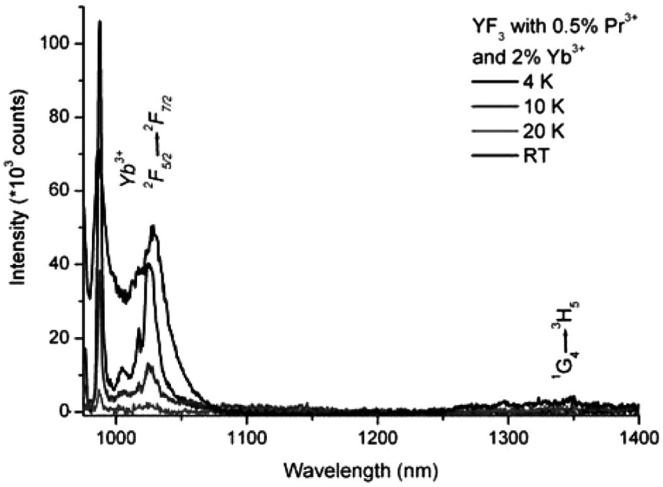

FIGURE 7 **Temperature dependent emission spectra for YF_3:Pr^{3+} (0.5%), Yb^{3+} (2%) for excitation into the Yb^{3+} $^2F_{5/2}$ level (950 nm).**

The peculiar temperature dependence can be explained by considering the two temperature regimes (4 to 50 K and 50 to 300 K, respectively). Upon raising the temperature from 4 to 50 K the energy transfer between neighboring Yb^{3+}-ions increases. Due to small energy differences between the local environment of lanthanide ions, the energy levels are at slightly different energies and resonant energy transfer is not possible. This hampers energy migration and as a result concentration quenching is reduced at 4 K and the $^2F_{5/2}$ emission is relatively strong. Upon raising the temperature, phonon-assisted energy transfer becomes possible and rapid energy migration to traps (including the $^1G_4$ level of Pr^{3+}) occurs, efficiently quenching the $^2F_{5/2}$ emission. When the temperature is raised further, thermally activated back-transfer from the $^1G_4$ level of Pr^{3+} becomes possible and as the temperature is raised, the back-transfer probability increases. The temperature regime where the increase in the Yb^{3+} emission is observed, is consistent with the energy difference between $^1G_4$ and $^2F_{5/2}$ ($\sim$300 cm^{-1}).

Support for the explanation for the temperature dependence of the emission intensities comes from temperature dependent luminescence decay curves. Energy migration and transfer of excitation energy from Yb^{3+} to the Pr^{3+} $^1G_4$ level also has an effect on the lifetimes of the Yb^{3+} $^2F_{5/2}$ emission. In Fig. 8 luminescence decay curves are shown at various temperatures between 4 and 300 K. The tail of the decay curves was fitted with a single exponential

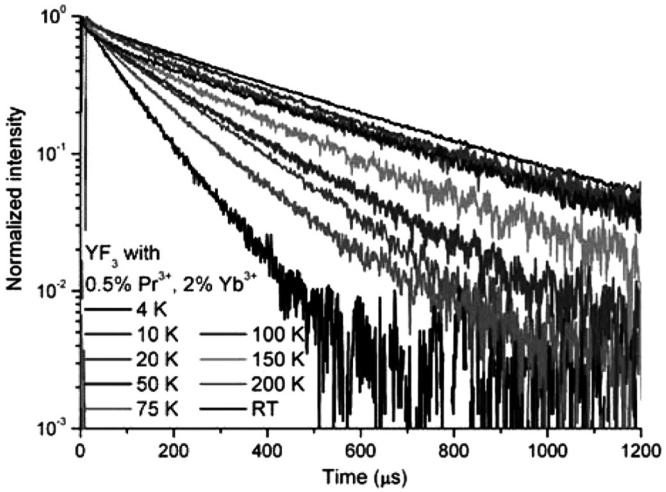

FIGURE 8 **Temperature dependent luminescence decay measurements for the Yb^{3+} $^2F_{5/2}$ emission (986 nm) in YF_3:Pr^{3+} (0.5%), Yb^{3+} (2%) after pulsed excitation into the Yb^{3+} $^2F_{5/2}$ level (950 nm).**

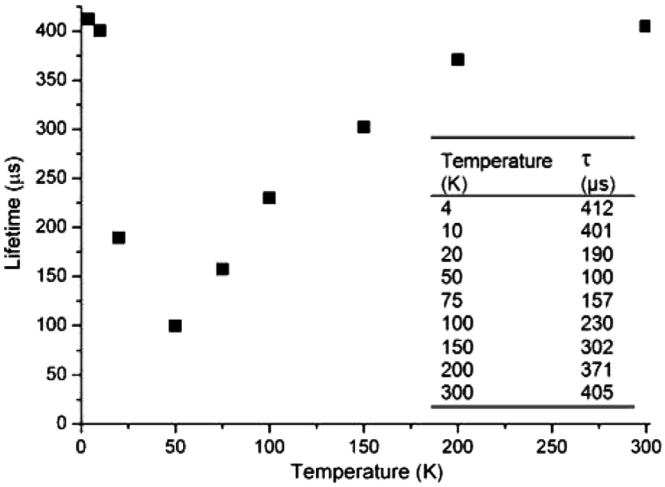

FIGURE 9 **Temperature dependence of the luminescence lifetimes deduced from single exponential fitting of the decay measurements of Yb^{3+} $^2F_{5/2}$ emission (986 nm) in YF_3:Pr^{3+} (0.5%), Yb^{3+} (2%) after excitation into the Yb^{3+} $^2F_{5/2}$ level (shown in Fig. 8).**

function and an average lifetime τ was determined for the Yb^{3+} $^2F_{5/2}$ emission and plotted as a function of temperature in Fig. 9. The luminescence lifetime at 4 K is approximately 410 μs and decreases to 100 μs as the temperature is increased to 50 K. When the temperature is increased further the lifetime starts to increase again, and at room temperature the lifetime is 405 μs, only slightly shorter than the lifetime at 4 K. The same trend was also observed for the sample doped with 0.5% Pr^{3+} and 5% Yb^{3+}. These results are consistent with the temperature dependence of the luminescence intensities and are explained by the temperature dependent energy transfer between the Yb^{3+} $^2F_{5/2}$ level and the Pr^{3+} $^1G_4$ level. As the temperature is raised from 4 to 50 K energy migration from Yb^{3+} to the Pr^{3+} $^1G_4$ level becomes more efficient, leading to a shortening of the lifetime for the Yb^{3+} $^2F_{5/2}$ emission. The Pr^{3+} $^1G_4$ level is some 300 cm^{-1} lower in energy than the Yb^{3+} $^2F_{5/2}$ level and is an efficient trap. The thermal energy at temperatures below 50 K is not sufficient to allow energy transfer from the Pr^{3+} $^1G_4$ level back to the Yb^{3+} $^2F_{5/2}$ level. At temperatures above 50 K thermally activated back-transfer starts to play a role and thermally activated transfer from Pr^{3+} $^1G_4$ to Yb^{3+} $^2F_{5/2}$ occurs. This process becomes more efficient at higher temperatures, leading to increasing lifetimes and higher intensity for the Yb^{3+} $^2F_{5/2}$ emission as the temperature is increased from 50 K to room temperature. The results on the temperature dependent luminescence and decay of the $^2F_{5/2}$ emission show that trapping of the excitation energy in the $^1G_4$ level of Pr^{3+} contributes to concentration quenching and can be reduced by raising the temperature and the Yb^{3+} concentration, promoting back-transfer to the $^2F_{5/2}$ level of Yb^{3+}. On the other, raising the Yb^{3+} concentration also induces faster energy migration to (other) traps which lowers the Yb^{3+} emission intensity. Optimization for the highest 1000 nm emission intensity will require optimizing the Pr^{3+} and Yb^{3+} concentration, as well as reducing the concentration of quenching centers by optimized synthesis procedures.

4. CONCLUSIONS

Downconversion of one blue-green photon to two NIR photons has been demonstrated in YF_3:Pr^{3+}, Yb^{3+} and takes place through two-step energy transfer from Pr^{3+} to Yb^{3+}. Room temperature emission and luminescence decay measurements show that the energy transfer efficiency increases with Yb^{3+} concentration, up to 86% for YF_3 doped with 0.5% Pr^{3+} and 30% Yb^{3+}. Comparison of the relative intensities for the $^3H_4 \rightarrow {}^3P_J$ to $^3H_4 \rightarrow {}^1D_2$ absorption/excitation lines in diffuse reflectance/excitation spectra confirms that downconversion is efficient for this lanthanide couple. Concentration quenching of the Yb^{3+} $^2F_{5/2}$ emission reduces the NIR output for Yb^{3+} concentrations which are needed to achieve efficient downconversion. Low temperature emission and luminescence decay measurements show that Pr^{3+} $^1G_4$ level plays an important role in the

energy transfer between Pr^{3+} and Yb^{3+} and the concentration quenching. Not only does energy transfer from Pr^{3+} to Yb^{3+} take place, but transfer of excitation energy from the Yb^{3+} $^2F_{5/2}$ level to the $^1G_4$ level of Pr^{3+} is also possible. This back-transfer quenches the Yb^{3+} emission around 1000 nm especially at low temperatures. Concentration quenching can be reduced by optimized synthesis conditions (to reduce the concentration of quenching centers related to defects or impurities), varying the concentration of Yb^{3+} and Pr^{3+} and choosing a system where the energy difference between the lowest $^1G_4$ level of Pr^{3+} and $^2F_{5/2}$ level of Yb^{3+} is as small as possible to reduce the trapping efficiency of $^1G_4$ level.

ACKNOWLEDGMENTS

This work is part of the Joint Solar Programme (JSP) of the Stichting voor Fundamenteel Onderzoek der Materie FOM, which is supported financially by Nederlandse Organisatie voor Wetenschappelijk Onderzoek (NWO). The JSP is co-financed by Gebied Chemische Wetenschappen of NWO and Stichting Shell Research. Financial support from the 'Energie Onderzoek Subsidie' (EOS) programme of SenterNovem, an agency of the 'Ministerie van Economische Zaken' of the Netherlands, is gratefully acknowledged.

REFERENCES

1. Trupke, T.; Green, M. A.; Würfel, P. Improving solar cell efficiency by down-conversion of high-energy photons. *J. Appl. Phys.* **2002**, *92*(3), 1668–1674.
2. Auzel, F. Upconversion and anti-Stokes processes with f and d ions in solids. *Chem. Rev.* **2004**, *104*(1), 139–173.
3. Piper, W. W.; De Luca, J. A.; Ham, F. S. Cascade fluorescent decay in Pr^{3+}-doped fluorides: achievement of a quantum yield greater than unity for emission of visible light. *J. Lumin.* **1974**, *8*(4), 344–348.
4. Srivastava, A. M.; Doughty, D. A.; Beers, W. W. Photon Cascade Luminescence of Pr^{3+} in $LaMgB_5O_{10}$. *J. Electrochem. Soc.* **1996**, *143*(12), 4113–4116.
5. Kück, S.; Sokólska, I.; Henke, M.; Scheffler, T.; Osiac, E. Emission and excitation characteristics and internal quantum efficiencies of vacuum-ultraviolet excited Pr^{3+}-doped fluoride compounds. *Phys. Rev. B* **2001**, *71*(16), 165112.
6. Wegh, R. T.; Donker, H.; Oskam, K. D.; Meijerink, A. Visible quantum cutting in $LiGdF_4:Eu^{3+}$ through downconversion. *Science* **1999**, *283*(5402), 663–666.
7. Vergeer, P.; Vlugt, T. J. H.; Kox, M. H. F.; den Hertog, M. I.; van der Eerden, J .P .J .M.; Meijerink, A. Quantum cutting by cooperative energy transfer in $Yb_xY_{1-x}PO_4:Tb^{3+}$. *Phys. Rev. B* **2005**, *71*, 014119.
8. Zhang, Q. Y.; Yang, G. F.; Jiang, Z. H. Cooperative downconversion in $GdAl_3(BO_3)_4:RE^{3+}$, Yb^{3+} (RE=Pr, Tb, and Tm). *Appl. Phys. Lett.* **2007**, *91*(5), 051903.
9. Yuan, J. L.; Zeng, X. Y.; Zhao, J. T.; Zhang, Z. J.; Chen, H. H.; Yang, X. X. Energy transfer mechanisms in Tb^{3+}, Yb^{3+} codoped Y_2O_3 downconversion phosphor. *J. Phys. D: Appl. Phys.* **2008**, *41*(10), 105406.
10. Lakshminarayana, G.; Yang, H.; Ye, S.; Liu, Y.; Qiu, J. Cooperative downconversion in $Pr^{3+}/Yb^{3+}:SiO_2$-Al_2O_3-BaF_2-GdF_3 glasses. *J. Mater. Res.* **2008**, *23*(11), 3090–3095.
11. Lakshminarayana, G.; Yang, H.; Ye, S.; Liu, Y.; Qiu, J. Cooperative downconversion in $Tm^{3+}/Yb^{3+}:SiO_2$-Al_2O_3-LiF-GdF_3 glasses. *J. Phys. D: Appl. Phys.* **2008**, *41*(17), 175111.
12. van der Ende, B. M.; Aarts, L.; Meijerink, A. Near-infrared quantum cutting for photovoltaics. *Adv. Mat.* **2009**, *21*(30), 3073–3077.
13. Bendall, P. J.; Catlow, C. R. A.; Corish, J.; Jacobs, P. W. M. Defect aggregation in anion-excess fluorites II. Clusters containing more than two impurity atoms. *J. Solid State Chem.* **1984**, *51*(2), 159–169.
14. Tallant, D. R.; Moore, D. S.; Wright, J. C. Defect equilibria in fluorite structure crystals. *J. Chem. Phys.* **1977**, *67*(6), 2897–2907.
15. Srivastava, A. M.; Duclos, S. J. On the luminescence of YF_3-Pr^{3+} under vacuum ultraviolet and X-ray excitation. *Chem. Phys. Lett.* **1997**, *275*(5–6), 453–456.
16. Peijzel, P. S.; Meijerink, A.; Reid, M. F.; Burdick, G. W. A complete $4f^n$ energy level diagram for all trivalent lanthanide ions. *J. Solid. State Chem.* **2005**, *178*(2), 448–453.
17. Judd, B. R. Optical absorption intensities of rare-earth ions. *Phys. Rev.* **1962**, *127* (3), 750–761; Ofelt, G. S. Intensities of crystal spectra of rare-earth ions. *J. Chem. Phys.* **1962**, *37*(3), 511–520.
18. De Mello Donegá, C.; Dirksen, G. J.; Folkerts, H. F.; Meijerink, A.; Blasse, G. The vibronic spectroscopy and luminescence concentration quenching of the Pr^{3+} ion in La_2O_3, LaOF and $LiYF_4$. *J. Phys. Chem. Solids* **1995**, *56*(2), 267–276.
19. Malinowski, M.; Joubert, M. F.; Jacquier, B. Dynamics of the IR-to-blue wavelength upconversion in Pr^{3+}-doped yttrium aluminum garnet and $LiYF_4$ crystals. *Phys. Rev. B.* **1994**, *50*(17), 12367–12374.